Journal of Alloys and Compounds 501 (2010) 115–119

Contents lists available at ScienceDirect

Journal of Alloys and Compounds

journal homepage: www.elsevier.com/locate/jallcom

High-temperature transport and thermoelectric properties of $Ca_3Co_{4-x}Ti_xO_9$

Luxiang Xu[a,*], Fang Li[b], Yang Wang[c,**]

[a] Lab for Low-dimensional Structure Physics, Institute of Solid State Physics and School of Physics and Electronic Engineering, Sichuan Normal University, No. 5 Jiang' an Road, Jinjiang District, Chengdu 610068, People's Republic of China
[b] School of Petroleum Engineering, Southwest Petroleum University, Xindu, Chengdu 610500, People's Republic of China
[c] Center for Condensed Matter Science and Technology (CCMST), Department of Physics, Harbin Institute of Technology, P.O. Box 3025, Science Park, No. 2 Yi-Kuang Street, Harbin 150001, People's Republic of China

ARTICLE INFO

Article history:
Received 15 December 2009
Received in revised form 6 April 2010
Accepted 7 April 2010
Available online 20 April 2010

Keywords:
$Ca_3Co_4O_9$
Doping
Thermoelectric properties
Electronic correlation

ABSTRACT

We report the high-temperature transport and thermoelectric properties of Co-site doped $Ca_3Co_{4-x}Ti_xO_9$ system. The results reveal that both resistivity and thermopower increase monotonously with Ti doping. When the relative Ti content is not more than $x = 0.2$, the substitution takes place in Ca_2CoO_3 sublayer; in contrast, if the relative Ti content reaches $x = 0.3$, the doped Ti ions may exist in both Ca_2CoO_3 and CoO_2 sublayers. As the Co ions in CoO_2 layer are substituted, the transport mechanism of the system varies, and the electronic correlation is pronounced enhanced. These changes induce a noticeable increase in thermopower. The figure of merit ZT value of $Ca_3Co_{3.7}Ti_{0.3}O_9$ is close to 0.3 at 1000 K, suggesting that Ti doped $Ca_3Co_4O_9$ series are promising thermoelectric oxides for high-temperature applications.

1. Introduction

Driven by the application as clean energy sources, environment-friendly thermoelectric materials that can convert heat energy into electrical energy directly via Seebeck effect and vice versa by Peltier effect have attracted much attention recently [1]. Generally, the efficiency of a thermoelectric material is described by a dimensionless figure of merit $ZT = S^2T/\rho\kappa$, where S, ρ, and κ are thermopower, resistivity, and thermal conductivity, respectively. $ZT > 1$ is required for practical thermoelectric applications. To date, only a few intermetallic compounds such as Bi_2Te_3, PbTe, and SiGe alloys exhibit high performance with $ZT > 1$, and these alloys remain the state-of-the-art thermoelectric materials [2]. Compared with the above mentioned thermoelectric alloys, metal oxides are more suitable for high-temperature thermoelectric applications because of their structural and chemical stabilities, oxidation resistance, and low-cost. The recent discoveries of large thermoelectric response in some 3d transition-metal oxides have attracted extensive interests in the study of thermoelectric oxides [3–6].

Among these transition-metal oxides, misfit-layered cobaltite $Ca_3Co_4O_9$ exhibits unusual thermoelectric characteristics: coexistence of a low resistivity and a large thermopower, and thus good thermoelectric performance [6]. Nevertheless, the intrinsic reasons for such a high thermoelectric performance remain puzzling, but the strong electronic correlation is considered to be crucial [3]. The crystal structure of $Ca_3Co_4O_9$ consists of two subsystems: distorted NaCl-type Ca_2CoO_3 sublattice and CdI_2-type CoO_2 sublattice alternatively stacking along the c-axis [6]. The electronic structure calculation indicates that the Fermi energy lies in the crystal-field gap of the d states in CoO_2 subsystem [7]. To optimize the thermoelectric performance of $Ca_3Co_4O_9$ system, many attempts have been made by choosing kinds of ions as dopants [8–19]. From these investigations, it is suggested that the substitutions of several rare-earth ions or Ag ion for Ca may efficiently improve the thermoelectric performance of $Ca_3Co_4O_9$.

Compared with the substitutions for Ca ions, doping in Co-site, particularly in CoO_2 layer, may result in more noticeable influence on the physical properties, because Co ions play an important role in magnetic interactions and the CoO_2 layer dominates the band structure and transport behavior [20–24]. For example, it has been reported that the substitution of Ti for Co changes the low-temperature electrical transport characteristics and induces an enhanced spin fluctuation together with spin glass behavior [23,24]. However, the effects of Ti doping on the thermoelectric properties remain unexplored. Very recently, we found the substitutions of transition-metal Fe, Mn, and Cu for Co cause several interesting influences on the strongly correlated properties and thermoelectric properties in $Ca_3Co_4O_9$ system [25,26]. Nong et al. investigated $Ca_3Co_{4-x}Ga_xO_9$ synthesized by hot-pressing and found that partial Ga substitution leads to a simultaneous increase in the electrical conductivity and thermopower [27]. This observed

* Corresponding author at: NIE 7-B3-05/06, Nanyang Walk 1, Singapore, Singapore.
** Corresponding author.
E-mail addresses: luxiang.xu@nie.edu.sg (L. Xu), wangyanghit@gmail.com (Y. Wang).

0925-8388/$ – see front matter © 2010 Elsevier B.V. All rights reserved.
doi:10.1016/j.jallcom.2010.04.055

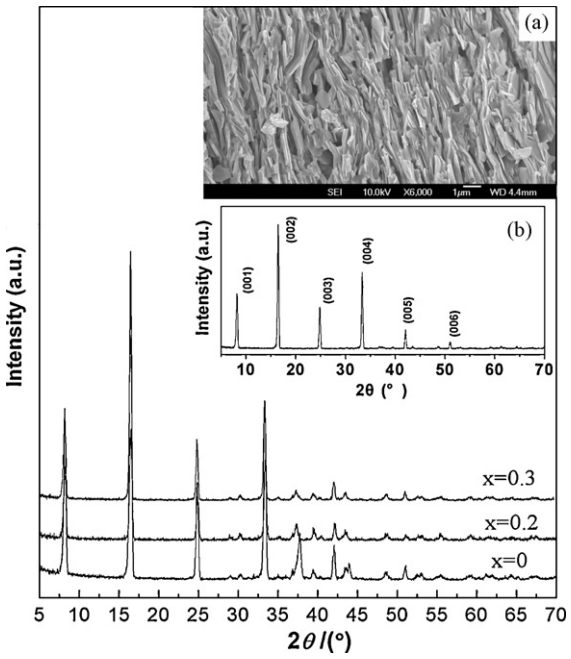

Fig. 1. X-ray powder diffraction patterns for the samples. The inset (a) shows the SEM micrograph for the cross section of the cold high-pressure fabricated $Ca_3Co_{3.7}Ti_{0.3}O_9$; the inset (b) shows the XRD pattern for the pressed surface of $Ca_3Co_4O_9$, in which (0 0 l) diffraction peaks are marked.

behavior is similar to that of Fe-doped $Ca_3Co_{4-x}Fe_xO_9$ [11]. In order to further investigate Co-site doped $Ca_3Co_4O_9$ system, in this paper, we report the effects of the substitution of Ti for Co on the high-temperature transport and thermoelectric properties of $Ca_3Co_4O_9$. The results reveal that the thermoelectric performance of $Ca_3Co_4O_9$ is efficiently enhanced by Ti doping.

2. Experimental

Polycrystalline $Ca_3Co_{4-x}Ti_xO_9$ (x = 0, 0.1, 0.2, and 0.3) were synthesized by solid state reaction followed by cold high-pressure process. Stoichiometric $CaCO_3$, Co_2O_3, and TiO_2 powders were mixed, pressed into pellets, and then sintered at 1173 K for 48 h under O_2 flow with intermediate grindings. Subsequently, the pellets were pulverized and cold-pressed into pellets under a high pressure of 3 GPa. Finally, the pellets were annealed under O_2 flow at 1173 K for 12 h and slowly cooled to room temperature. X-ray diffraction (XRD) measurement was performed using the XRD diffractometer (D8 Advanced) with Cu Kα radiation. The microstructure was observed with a JEOL JSM-6700F scanning electron microscope (SEM). Resistivity from room temperature to 1000 K was measured by a standard four-probe method using the 2400 SourceMeter (KEITHLEY). Thermopower was calculated from the thermoelectric voltage and the temperature gradient across the samples (ULVAC-RIKO: ZEM-3). Thermal conductivity was calculated by $\kappa = DC_p d$, where D is thermal diffusivity (measured by a laser flash method, Netzsch LFA-457), C_p is specific heat capacity (determined by Netzsch DSC-404), and d is the material density. The low-temperature Hall effect and specific heat were measured using the physical property measurement system (Quantum Design: PPMS).

3. Results and discussion

As shown in Fig. 1, the XRD patterns of the crushed powder of the samples are identical to the standard JCPDS card (21-139), indicating that single-phase $Ca_3Co_{4-x}Ti_xO_9$ series were successfully synthesized. Compared with the $Ca_3Co_4O_9$ parent, the 2θ angles of diffraction peaks in the XRD patterns of the doped samples shift slightly, mainly due to the different ionic radii between Co and Ti ions. It should be noted that compared with the XRD patterns of the crushed powder and JCPDS card, the XRD profile for the pressed surface of samples exhibits strong diffraction peaks from (0 0 l) planes, while other diffraction peaks are quite weak [see the inset (b) of Fig. 1]. This indicates the high-textured structure characteristic in these ceramic specimens. Generally, the degree of crystallographic anisotropy of a material can be evaluated in terms of the Lotgering factor f [28], $f = (p - p_0)/(1 - p_0)$, where $p = \sum I(00l)/\sum I(hkl)$, and $p_0 = p$ for a randomly oriented sample. When the c-axis directions of grains are completely aligned along the pressing direction, the f value should equal 1. The values of f of (0 0 l) planes for these cold highly pressed samples are around 0.88, implying their large crystallographic anisotropy. One can see that when the specimens were pulverized, the diffraction peaks from other planes appear, but the relative intensity of the peaks for the powder XRD is still different from that of JCPDS card. The Lotgering factor f of the powder was calculated to be around 0.65, which indicates that the high texture was partly destroyed after pulverizing, but the crystallographic anisotropy of the grains still exists in the samples. The SEM image of the sample clearly indicates the high-textured structure of these samples synthesized by cold high pressure [see the inset (a) of Fig. 1]. Most grains exhibit a plate-like shape and are preferentially aligned along the pressing direction, exhibiting a quasi-two-dimensional layered crystal structure.

The temperature dependences of resistivity ρ and thermopower S of the samples from room temperature up to 1000 K are presented in Fig. 2. One can see that Ti doping does not change the shapes of ρ–T and S–T curves in the main, but doping enhances ρ and S gradually. Additionally, the sudden metal–semiconductor (MS) transition around 380 K in the ρ–T curve for undoped $Ca_3Co_4O_9$ becomes unconspicuous with doping; only a broad peak in the range of 300–400 K in ρ–T curves is shown, and the MS transition temperature T_{MS} lowers gradually. The increase in the values of ρ with doping can be attributed to the decrease of carrier concentration n of the system, as confirmed by the Hall coefficient measurements (see Fig. 3). The variations of resistivity by Ti doping are similar to the reported low-temperature results of $Ca_3Co_{4-x}Ti_xO_9$ single crystals [23,24]. Because the majority charge carriers of $Ca_3Co_4O_9$ system are holes [6], and the valence of Ti ion is higher than the average valence of Co in $Ca_3Co_4O_9$, the substitution of Ti for Co can actually be considered as electron-doping and thus reduce the hole concentration. As a result, ρ increases monotonously with doping.

In $Ca_3Co_4O_9$ system, S can be expressed by

$$S(T) = \frac{c_e}{n} + \frac{\pi^2 k_B^2 T}{3e}\left[\frac{\partial \ln \mu(\varepsilon)}{\partial \varepsilon}\right]_{\varepsilon=\varepsilon_F}, \quad (1)$$

where $\mu(\varepsilon)$ and c_e are energy ε correlated carrier mobility and electronic specific heat [24,29]. The first term of Eq. (1) is dominant, similar to the simple Drude picture $S \sim c_e/n$ [30], so the increase in S by Ti doping can also be explained by the decrease in carrier concentration n. However, we notice that S of the x = 0.3 sample exhibits a noticeable increase that cannot be quantitatively interpreted by the variation of carrier concentration. In order to elucidate this phenomenon, next we discuss the transport behavior of the $Ca_3Co_{4-x}Ti_xO_9$ system.

It is well known that the hopping conduction behavior exists in $Ca_3Co_4O_9$ at high temperature [9,10], namely electric conductivity σ can be expressed by

$$\sigma = \frac{\sigma_0}{T}\ \exp\left(-\frac{E_a}{k_B T}\right), \quad (2)$$

where σ_0 is a constant and E_a denotes activation energy. As shown in Fig. 4(a), the plots of $\ln(\rho/T)$ versus $1/T$ for the x = 0–0.2 samples lie on straight lines above ~600 K, indicating the hopping conduction mechanism at higher temperature range in these samples. The substitution of Ti for Co does not change the transport mechanism, but the hopping activation energy E_a, obtained from the slopes of the linear fitting, increases slightly. In contrast, the x = 0.3 sample does not obey such a transport mechanism in the whole measured temperature range; instead its ρ–T curve can be fitted by Mott's

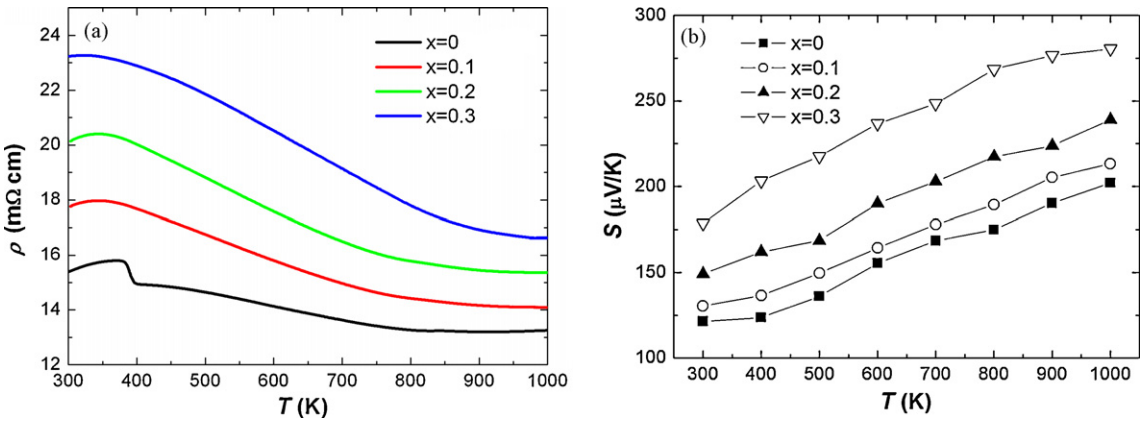

Fig. 2. Temperature dependences of resistivity ρ and thermopower S for the samples.

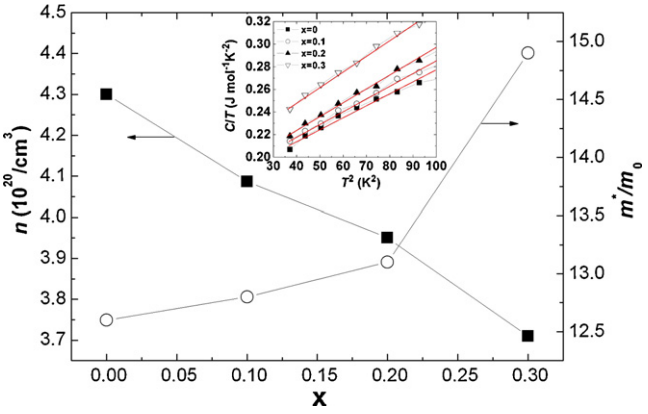

Fig. 3. Room-temperature carrier concentration n and electronic effective mass m^* as a function of doping level x for the samples; m_0 denotes the rest mass of electrons. The inset presents the temperature dependence of specific heat C for the samples plotted as C/T versus T^2 with the fitted lines.

two-dimensional variable range hopping (2D-VRH) model, viz.

$$\rho = \rho_0 \exp\left(\frac{T_0}{T}\right)^{1/3}, \quad (3)$$

where ρ_0 is a constant, $T_0 \sim 1/[k_B N(\varepsilon_F) l_v^2]$ means the VRH characteristic temperature associated with the density of localized states at Fermi energy $N(\varepsilon_F)$, and l_v is the localization length [see Fig. 4(b)] [31]. Such phenomena are reminiscent of the behavior found in Co-site Ni, Fe, Mn etc doped $Ca_3Co_4O_9$ and Co-site Cu etc doped $NaCo_2O_4$ in which there is only one kind of Co-site: CoO_2 layer [10,32,33]. The variations of transport properties in the $x = 0.3$ sample are similar to those of $Ca_3Co_{4-x}(Fe/Mn)_xO_9$ where the Co ions in CoO_2 layer are substituted and those of $NaCo_{1-x}Cu_xO_2$ [25,32,33]. Therefore, we speculate that when the relative content of doped Ti is not more than 0.2, the Ti ions mainly replace the Co ions in Ca_2CoO_3 layer; if the relative Ti content reaches 0.3, because of the solubility limit, in addition to the substitution for Co in Ca_2CoO_3 layer, several Ti ions may replace the Co ions in CoO_2 layer. Since the CoO_2 layer dominates the transport behavior of $Ca_3Co_4O_9$ system, the substitution in Ca_2CoO_3 layers has little influence on the transport mechanism. However, if the substitution takes place in CoO_2 layers, that can not only produce strong disorder and distortion, but also change the transport mechanism because the conduction path in CoO_2 layer is disturbed. When the strong distortion and disorder in CoO_2 layers are induced by heavier doping, the hole hopping tends towards farther low-energy sites rather than neighbor sites, and consequently the VRH mechanism dominates. Moreover, due to the anisotropic layered structure, the VRH transport is two-dimensional. It should be emphasized that the VRH mechanism can be only achieved when the thermally activated energy is not enough to make holes hopping to near neighbor sites, so that the VRH mechanism first locates at lower temperature range. As for the high-temperature range, the energy of hole is relatively high; in this case the VRH may not be the unique transport mechanism. That is why the $\ln\rho$ versus $1/T^{1/3}$ plot in $Ca_3Co_{3.7}Ti_{0.3}O_9$ keeps linear at low-temperature region but the linear relationship gradually deviates at high-temperature region.

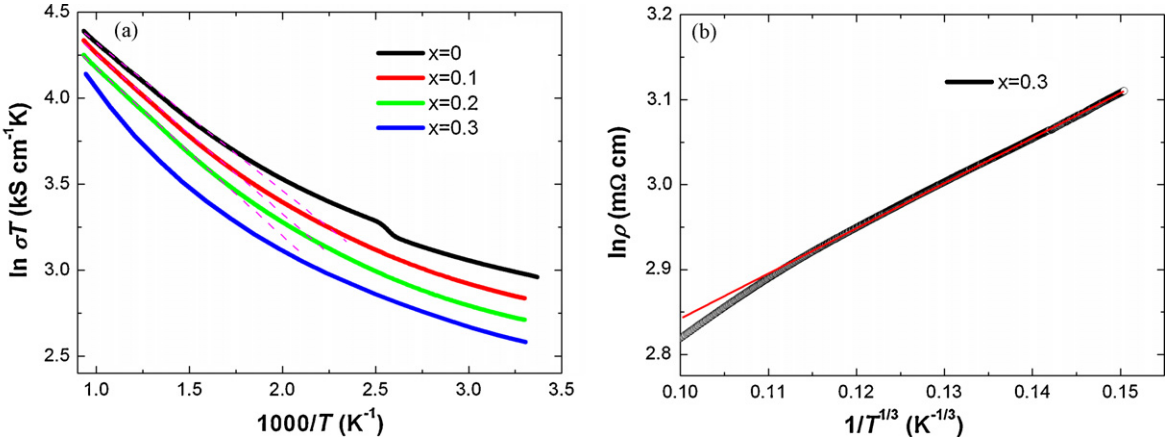

Fig. 4. (a) Plot of $\ln(\rho/T)$ versus $1/T$ for the samples; the red lines denote the linear fitting. (b) 2D-VRH fitting for the $x = 0.3$ sample. (For interpretation of the references to color in this figure legend, the reader is referred to the web version of this article.)

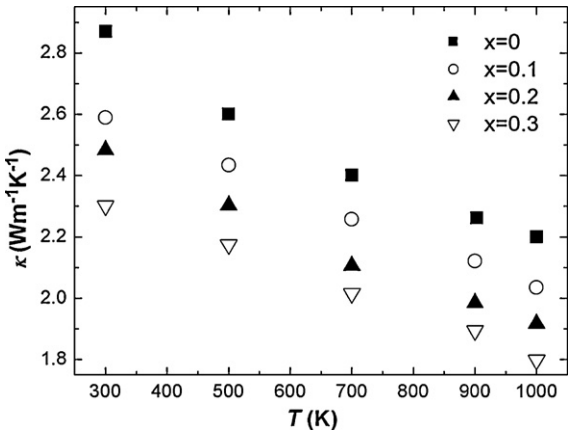

Fig. 5. Temperature dependence of thermal conductivity κ for the samples.

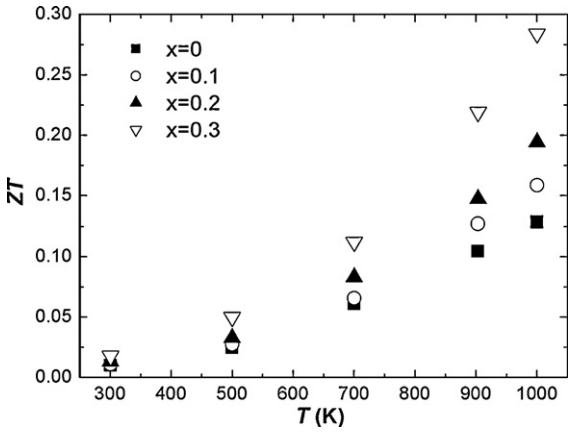

Fig. 6. Temperature dependence of ZT for the samples.

On the other hand, because the Fermi level lies in the crystal-field gap of the d states in the CoO_2 layer as mentioned above [7], doping in CoO_2 layer may vary the band structure of the system. The specific heat measurements revealed the enhanced electronic correlation in the $x = 0.3$ sample. Temperature dependence of specific heat C in a low-temperature range can be written as $C/T \sim \gamma + \beta T^2$, where γ is electronic specific heat coefficient. One can see from the inset of Fig. 3 that γ increases slightly at $x \leq 0.2$, but increases obviously for $x = 0.3$. This implies the remarkable enhancement of electron effective mass m^* and the electronic correlation. The enhanced electronic specific heat can also contribute to the increase in S according to $S \sim c_e/n$, so the observed increase in S in $Ca_3Co_{3.7}Ti_{0.3}O_9$ results from the decrease in carrier concentration together with the increase in electronic correlation. From these results, one can see that doping in different sublayers in $Ca_3Co_4O_9$ may give rise to different influences on the physical properties. Nevertheless, more direct evidence that in which sublayer the Co ions are substituted still needs further study. The change in electronic specific heat with doping can be correlated with the variation of bandwidth. Ti doping decreases carrier concentration, which increases the average distance between holes. In a strongly correlated system, the increase in the average distance between carriers will reduce bandwidth and enhance electronic correlations. Consequently, electron effective mass and electronic specific heat increase. Furthermore, the increase in the average distance between carriers also means the localization of system increases, which suggests that a semiconducting state is more stable. Therefore, T_{MS} in the ρ–T curves gradually decreases with doping.

The temperature dependence of thermal conductivity κ of the sample is shown in Fig. 5. For all samples, κ monotonously decreases as temperature increases. Ti doping gradually lowers κ. The total thermal conductivity can be expressed by the sum of phonon thermal conductivity κ_{ph} and carrier thermal conductivity κ_{car}, i.e. $\kappa = \kappa_{ph} + \kappa_{car}$. Estimated from Wiedemann–Franz's law that $\kappa_{car} = L_0 T/\rho$ where $L_0 = \pi^2 k_B^2/3e^2$ is Lorentz constant, κ_{car} is less than 10% of κ for all samples. Accordingly, κ_{ph} is the predominant component in κ, and the variation of κ mainly arises from the alteration of κ_{ph}. Because the doped Ti ions induce disorder and structural distortion, which can bring the lattice disharmony and hence strongly scatter phonons, so the phonon transport is suppressed and thus κ decreases.

Fig. 6 presents the ZT values of the samples. Although S and ρ both increase by Ti doping, ZT is efficiently improved. ZT monotonously increases as temperature rises. For $Ca_3Co_{3.7}Ti_{0.3}O_9$, owing to the remarkable increase in S along with the decrease in κ, the ZT is close to 0.3 at 1000 K, which is a quite high value among ceramic oxides. This result indicates that the thermoelectric performance of $Ca_3Co_4O_9$ is successfully improved by Ti doping.

4. Conclusions

A series of high-textured Co-site Ti doped $Ca_3Co_4O_9$ samples were fabricated by cold high-pressure method, and their thermoelectric properties were investigated from room temperature up to 1000 K. The results indicate that when the Ti content reaches 0.3, Ti ions may exist in both CoO_2 and Ca_2CoO_3 sublayers. Because the CoO_2 layer is disturbed, the transport mechanism varies from thermally activated hopping to 2D-VRH. The electronic correlation is pronounced enhanced in $Ca_3Co_{3.7}Ti_{0.3}O_9$, which induced an observed increase in thermopower. Thermal conductivity monotonously decreases with doping. As a result, the ZT value of $Ca_3Co_{3.7}Ti_{0.3}O_9$ is close to 0.3 at 1000 K, indicating that the thermoelectric performance of $Ca_3Co_4O_9$ system is efficiently improved by Ti doping and $Ca_3Co_{4-x}Ti_xO_9$ series may be promising thermoelectric oxides for high-temperature applications.

Acknowledgement

The author Luxiang Xu acknowledges the financial support of Natural Science Foundation of Sichuan Provincial Education Department (Grant No. 2006C020).

References

[1] L.E. Bell, Science 321 (2008) 1457.
[2] G.J. Snyder, E.S. Toberer, Nat. Mater. 7 (2008) 105.
[3] P. Limelette, V. Hardy, P. Auban-Senzier, D. Jérome, D. Flahaut, S. Hébert, R. Frésard, Ch. Simon, J. Noudem, A. Maignan, Phys. Rev. B 71 (2005) 233108.
[4] H. Ohta, K. Sugiura, K. Koumoto, Inorg. Chem. 47 (2008) 8429.
[5] D. Flahaut, T. Mihara, R. Funahashi, N. Nabeshima, K. Lee, H. Ohta, K. Koumoto, J. Appl. Phys. 100 (2006) 084911.
[6] A.C. Masset, C. Michel, A. Maignan, M. Hervieu, O. Toulemonde, F. Studer, B. Raveau, J. Hejtmanek, Phys. Rev. B 62 (2000) 166.
[7] R. Asahi, J. Sugiyama, T. Tani, Phys. Rev. B 66 (2002) 155103.
[8] G.J. Xu, R. Funahashi, M. Shikano, I. Matsubara, Y.Q. Zhou, Appl. Phys. Lett. 80 (2002) 3760.
[9] Y. Wang, Y. Sui, J.G. Cheng, X.J. Wang, J.P. Miao, Z.G. Liu, Z.N. Qian, W.H. Su, J. Alloys Compd. 448 (2008) 1.
[10] Q. Yao, D.L. Wang, L.D. Chen, X. Shi, M. Zhou, J. Appl. Phys. 97 (2005) 103905.
[11] C.J. Liu, L.C. Huang, J.S. Wang, Appl. Phys. Lett. 89 (2006) 204102.
[12] Y. Wang, Y. Sui, J.G. Cheng, X.J. Wang, W.H. Su, J. Phys. D: Appl. Phys. 41 (2008) 045406.
[13] J. Pei, G. Chen, D.Q. Lu, P.S. Liu, N. Zhou, Solid State Commun. 146 (2008) 283.
[14] Y. Wang, Y. Sui, J.G. Cheng, X.J. Wang, W.H. Su, J. Alloys Compd. 477 (2009) 817.
[15] F.P. Zhang, Q.M. Lu, J.X. Zhang, J. Alloys Compd. 484 (2009) 550.
[16] H.Q. Liu, Y. Song, S.N. Zhang, X.B. Zhao, F.R. Wang, J. Phys. Chem. Solids 70 (2009) 600.
[17] F.P. Zhang, Q.M. Lu, J.X. Zhang, X. Zhang, J. Alloys Compd. 477 (2009) 543.
[18] H.Q. Liu, X.B. Zhao, T.J. Zhu, Y. Song, F.P. Wang, Curr. Appl. Phys. 9 (2009) 409.

[19] G.D. Tang, Z.H. Wang, X.N. Xu, L. Qiu, Y.W. Du, J. Appl. Phys. 107 (2010) 053715.
[20] J. Sugiyama, C. Xia, T. Tani, Phys. Rev. B 67 (2003) 104410.
[21] J. Sugiyama, H. Itahara, T. Tani, J.H. Brewer, E.J. Ansaldo, Phys. Rev. B 66 (2002) 134413.
[22] J. Sugiyama, J.H. Brewer, E.J. Ansaldo, H. Itahara, K. Dohmae, Y. Seno, C. Xia, T. Tani, Phys. Rev. B 68 (2003) 134423.
[23] B.C. Zhao, Y.P. Sun, W.H. Song, J. Appl. Phys. 99 (2006) 073906.
[24] B.C. Zhao, Y.P. Sun, W.J. Lu, X.B. Zhu, W.H. Song, Phys. Rev. B 74 (2006) 144417.
[25] Y. Wang, Y. Sui, P. Ren, L. Wang, X.J. Wang, W.H. Su, H.J. Fan, Chem. Mater. 22 (2010) 1155.
[26] Y. Wang, Y. Sui, X.J. Wang, W.H. Su, X.Y. Liu, J. Appl. Phys. 107 (2010) 033708.
[27] N.V. Nong, C.J. Liu, M. Ohtaki, J. Alloys Compd. 491 (2010) 53.
[28] F.K. Lotgering, J. Inorg. Nucl. Chem. 9 (1959) 113.
[29] T. Takeuchi, T. Kondo, T. Takami, H. Takahashi, H. Ikuta, U. Mizutani, K. Soda, R. Funahashi, M. Shikano, M. Mikami, S. Tsuda, T. Yokoya, S. Shin, T. Muro, Phys. Rev. B 69 (2004) 125410.
[30] N.W. Ashcroft, N.D. Mermin, Solid State Physics, HoltSaunders, Philadelphia, PA, 1976.
[31] N.F. Mott, A. Davis, Electronic Processes in Non-Crystalline Materials, Clarendon, Oxford, 1979.
[32] M. Ito, T. Nagira, Y. Oda, S. Katsuyama, K. Majima, H. Nagai, Mater. Trans. 43 (2002) 601.
[33] I. Terasaki, Y. Ishii, D. Tanaka, Y. Iguchi, Jpn. J. Appl. Phys. 40 (Part 2) (2001) L65.